



Three Robust Edges Stopping Functions For Image Denoising

Hicham Rezgui, Messaoud Maouni, Mohammed Lakhdar Hadji and Ghassen Touil

ABSTRACT: In this paper, we present three strong edge stopping functions for image enhancement. These edge stopping functions have the advantage of effectively removing the image noise while preserving the true edges and other important features. The obtained results show an improved quality for the restored images compared to existing restoration models.

Key Words: Perona-Malik model, Edge stopping function, Image denoising and restoration, Numerical approximation.

Contents

1 Introduction	1
2 Edges Stopping Functions	2
3 The proposed edge stopping functions	3
3.1 Description of the proposed edge stopping functions	3
4 Numerical Approximation	4
4.1 Criterias of Performance	4
5 Results and Comparison Approach	5
6 Conclusion	11

1. Introduction

Given the importance of the images taken in our daily life, their quality became so important in many engineering applications. Images are subject to different kinds of distortions resulting in different levels of degradations. The noise is obtained either from the equipment used in the imaging or during transmission. In the past 30 years, researchers have relied on second-order partial differential equations to find ways to eliminate the image noise while preserving their original structure and fine details. One of these methods is "linear filtering". The basic idea behind this method is to eliminate noise in all directions with the same rate of diffusion. As a consequence, it is not possible to maintain image structures such as edges and fine structures. The researchers then resorted to the nonlinear anisotropic method that was first identified by Perona and Malik in 1990 [9] in which the diffusion process is stopped before reaching the edges, resulting in a better preservation of the edges. Perona and Malik obtained these results by introducing a key point: using an edge stopping function to control the diffusion process so that the form of the linear filter was modified as described below:

$$\frac{\partial u}{\partial t} = \text{div}(g(\|\nabla u\|)\nabla u),$$

The suggested nonlinear model is said to be able to preserve and enhance image edges while simultaneously removing noise. A lot of work has been done since then. In 1990, Rudin and Osher tried to improve the time-reverse heat equation using a shock filter [11]. Catté et al. [1] proposed a modified version of PM model in 1992 in which the diffusion is guided by the intensity of the gradients. Black et al., proposed an edge stopping function based on Tukey's biweight robust estimator [8]. Later on in 2011 Tian et al. [2] proposed a new denoising method by performing an iterative texture-based eigenvalue analysis approach.

2010 *Mathematics Subject Classification:* 35XX, 35RXX.

Submitted December 20, 2018. Published April 05, 2019

A directional Laplacian-based PM filter was proposed by Wang et al. in 2013. It is claimed to be able to remove gradient impact and can maintain acute edges [17]. Chen et al., proposed in 2013 an edge preserving image denoising with a closed form solution [12]. Liu et al. suggested in 2014 an adaptative anisotropic diffusion filter based on a frame tensor while a time-dependent anisotropic diffusion image smoothing method was proposed in [6]. Barbu proposed in 2014 a robust anisotropic diffusion scheme for removing image noise [13]. Finally, Kamalaveni et al. suggested in 2015 an image denoising technique using a variation of PM model with different edge stopping functions [15].

This paper is organized as follows. In section 2, a review of recent work based on edge stopping functions for image restoration is presented. In section 3, three new edges stopping functions based on the convolution of a two-dimensional Gaussian filter with the local gradient of the image are detailed. Numerical approximation of the proposed models is presented in section 4. The comparison approach is presented with the main results of the present work in section 5 along with an evaluation of the proposed filters using a set of original images. Finally, a conclusion is given with the references in the last section.

2. Edges Stopping Functions

The two following edge stopping functions were first suggested by Perona and Malik: $g_1(\|\nabla u\|) = \frac{1}{1 + (\frac{\|\nabla u\|}{k})^2}$ and $g_2(\|\nabla u\|) = e^{-\left(\frac{\|\nabla u\|}{k}\right)^2}$, where k is the gradient magnitude threshold parameter. Perona and Malik imposed that each of the functions g_1 and g_2 satisfies the two following conditions: $\lim_{\|\nabla u\| \rightarrow \infty} g_i(\|\nabla u\|) = 0$ and $\lim_{\|\nabla u\| \rightarrow 0} g_i(\|\nabla u\|) = 1$ for $i = 1, 2$.

This kind of functions has a central role in the anisotropic diffusion model. It must be a monotonous decreasing function. If the image gradient is greater than the threshold coefficient, the edge stopping function slowly tends to zero, thereby protecting the image edges while eliminating the noise. If the image gradient is smaller than the threshold parameter, the edge stopping function tends to 1. Thus, an anisotropic filter transforms into a linear filter called the heat equation, resulting in erosion of the image edges and smoothing the fine structures. For this reason, the performance of the anisotropic diffusion is based on the judicious choice of a threshold parameter and an edge stopping function is therefore of great importance in image processing. Variations of the original model proposed by Perona and Malik were suggested later on new edge stopping functions were used in literature for image restoration. Edge stopping functions for image restoration will be presented in this section. Based on the previously mentioned work of Catté et al., Whitaker and Pizer [10] used a decreasing scaling function of time t instead of the scaling parameter $\sigma(t)$ is given by the following expression: $\sigma(t) = \sigma_0 - \alpha t$ or $\sigma(t) = \sqrt{\sigma_0^2 - 2\alpha t}$, where σ_0 is a constant and α is a constant that controls the decrease of the scaling parameter. Li and Chen [16] focused on the magnitude of the local gradient k of the same work of Catté et al., they suggested k as a decreasing function of the number of iterations t .

Black et al. [8] proposed a new edge stopping function defined by:

$$c(\|\nabla u\|) = \begin{cases} \frac{1}{2} \left[1 - \left(\frac{\|\nabla u\|}{s} \right)^2 \right]^2, & \text{if } \|\nabla u\| \leq s \\ 1, & \text{otherwise,} \end{cases}$$

where $s = \sqrt{2}k$.

Monteil and Beghdadi presented a new interpretation and improvement of the nonlinear anisotropic diffusion for image enhancement [3], proposing a new edge stopping function:

$$c(\|\nabla u\|) = \frac{1}{2} [\tanh(\gamma(k - \nabla u(x, y, t))) + 1],$$

where γ controls the steepness of the min-max transition region and k is the gradient magnitude threshold parameter.

Weickert [4] proposed a novel edge stopping function defined by:

$$c(\|\nabla u\|) = \begin{cases} 1 - e^{-3,31488 \times \left(\frac{k}{\|\nabla u\|}\right)^8}, & \text{if } \|\nabla u\| \neq 0 \\ 1, & \text{otherwise,} \end{cases}$$

Guo et al. [19] proposed an adaptive PM model based on a new edge stopping function given by:

$$c(\|\nabla u\|) = \frac{1}{\left(1 + \left(\frac{\|\nabla u\|}{k}\right)^{\alpha(\|\nabla u\|)}\right)},$$

where

$$\alpha(\|\nabla u\|) = 2 - \frac{2}{\left(1 + k \|\nabla G_\sigma * u\|^2\right)}.$$

Barbu [13] suggested a robust anisotropic diffusion scheme given by:

$$g_{k(u)}(\|\nabla u\|) = \begin{cases} \alpha \sqrt{\frac{k(u)}{\beta \times s^2 + \gamma}}, & \text{if } s > 0 \\ 1, & \text{if } s \neq 0, \end{cases}$$

where $\alpha, \beta \in [0.5; 0.8]$, $\gamma \in [0.5; 5]$ and $k(u) = \frac{\text{median}(u)}{\varepsilon \eta(u)} \|u\|_F$, $\varepsilon \in (0; 1]$ and $\|u\|_F$ is the Frobenius norm of image u , $\text{median}(u)$ represents its median value and $\eta(u)$ is the number of its pixels. Barbu and Moroşanu [14] proposed a novel nonlinear second-order parabolic PDE based on an edge stopping function ζ_u given by the following expression:

$$\zeta_u(s) = \xi \sqrt{\frac{\gamma(u)}{\beta \ln(s + \gamma(u))^3 + \delta}},$$

where $\gamma(u) = \alpha \cdot \mu(\|u\|) + \eta \cdot \text{pos}(u)$, whereas $\alpha, \beta, \delta, \eta, \xi \in (0; 3]$, μ returns the average value and $\text{pos}(u)$ gets the position of u in the evolving sequence.

3. The proposed edge stopping functions

In this section, our three edge stopping functions are presented. The essential goal of this work is to allow an efficient processing of images that successfully removes noise while preserving image edges and fine features. The proposed edge stopping functions satisfy both conditions: they are positive and non-increasing. The diffusion rate of those functions is high in homogenous regions, ie., if the norm of the image edge tends to zero, the diffusion rate is the highest possible but it is low within textured regions. Furthermore, the magnitude of the diffusion parameter has an important role in adjusting the diffusion rate; in other words, it plays a key role in preserving the correct edges of the image. The improved nonlinear problem of PM is defined as follows:

$$\frac{\partial I}{\partial t} = \text{div}(H_m(\|G_\sigma * \nabla I\|)\nabla I), \text{ for } m = 1, 2, 3$$

where G_σ is a two-dimensional Gaussian filter while σ is the scale parameter.

3.1. Description of the proposed edge stopping functions

The edge stopping functions have an important role in image denoising, as the performance of each function differs from one to another. Our edge stopping functions are denoted respectively as follows: H_1 denotes the first edge stopping function, it is given by:

$$H_1(\|G_\sigma * \nabla I\|) = \left(\frac{3}{2} - \frac{3}{2 + 4e^{-\left(\frac{\|G_\sigma * \nabla I\|}{R}\right)^2}} \right),$$

where R is the gradient magnitude threshold parameter.

We notice that H_1 tends to zero when the gradient is high and the performance is very high in homogeneous regions. In a mathematical sense, $\lim_{s \rightarrow +\infty} H_1(s) = 0$ and $\lim_{s \rightarrow 0} H_1(s) = 1$. It can be clearly seen the better denoising results of H_1 in Figures 1, 2, 3, 4, 5 and 8 below.

The second edge stopping function H_2 is defined as follows:

$$H_2(\|G_\sigma * \nabla I\|) = 1 - \left(1 - \log \left(1 + \frac{(\|G_\sigma * \nabla I\| + 1)^{\frac{1}{4}}}{1 + \left(\frac{\|G_\sigma * \nabla I\|}{R}\right)^4} \right) \right)^{\frac{5}{1 + \frac{\|G_\sigma * \nabla I\|}{R}}},$$

this function could be used for processing textured and medical images, where it showed a greater potential to eliminate the noise of images and to enhance the true image edges while maintaining the small features. The effectiveness of H_2 is also proved by the accurate noise discrimination on the true image edges. The results are shown below in Figure 1, 2, 3, 4, 6 and 8.

The third edge stopping function H_3 is defined as follows:

$$H_3(\|G_\sigma * \nabla I\|) = \left(1 - \tanh \left(\frac{\|G_\sigma * \nabla I\|}{R} \right) \right)^2 \Bigg|^4.$$

By applying the function H_3 , we obtained better denoising results which are reflected in Figure 1, 2, 3, 4, 7 and 8 below. Furthermore, function H_3 reduces the staircasing effect in the resulting image and discriminates the noise on true edges without removing them.

4. Numerical Approximation

The implementation of our edge stopping functions passes through solving a nonlinear diffusion problem using the Euler forward finite difference scheme. The method is described in what follows:

$$I_{i,j}^{n+1} = I_{i,j}^n + \Delta t \times \left[\begin{array}{l} H_m(\|\nabla^N I_{i,j}^n\|) \nabla^N I_{i,j}^n + H_m(\|\nabla^S I_{i,j}^n\|) \nabla^S I_{i,j}^n + \\ H_m(\|\nabla^E I_{i,j}^n\|) \nabla^E I_{i,j}^n + H_m(\|\nabla^W I_{i,j}^n\|) \nabla^W I_{i,j}^n + \\ H_m(\|\nabla^{NE} I_{i,j}^n\|) \nabla^{NE} I_{i,j}^n + H_m(\|\nabla^{NW} I_{i,j}^n\|) \nabla^{NW} I_{i,j}^n + \\ H_m(\|\nabla^{SE} I_{i,j}^n\|) \nabla^{SE} I_{i,j}^n + H_m(\|\nabla^{SW} I_{i,j}^n\|) \nabla^{SW} I_{i,j}^n \end{array} \right]$$

for $m = 1, 2, 3$, where n is the number of iterations, $\|\cdot\|$ is the Euclidean norm and Δt is time step, whereas N, S, E, W, NE, NW, SE and SW (North, South, East, West, NorthEast, NorthWest, SouthEast and SouthWest) represent local gradient directions. The local gradient is accounted using eight neighboring directions as follows:

$$\begin{aligned} \nabla^N I_{i,j}^n &= I_{i-1,j}^n - I_{i,j}^n & \nabla^E I_{i,j}^n &= I_{i,j+1}^n - I_{i,j}^n \\ \nabla^S I_{i,j}^n &= I_{i+1,j}^n - I_{i,j}^n & \nabla^W I_{i,j}^n &= I_{i,j-1}^n - I_{i,j}^n \\ \nabla^{NW} I_{i,j}^n &= \frac{I_{i-1,j-1}^n - I_{i,j}^n}{2} & \nabla^{NE} I_{i,j}^n &= \frac{I_{i-1,j+1}^n - I_{i,j}^n}{2} \\ \nabla^{SE} I_{i,j}^n &= \frac{I_{i+1,j+1}^n - I_{i,j}^n}{2} & \nabla^{SW} I_{i,j}^n &= \frac{I_{i+1,j-1}^n - I_{i,j}^n}{2} \end{aligned}$$

The implementation results of the proposed functions are compared using different performance metrics. The detailed description is presented in what follows.

4.1. Criterias of Performance

Several performance metrics are available to measure the quality of denoised images. Three widely used metrics were investigated in the present study. These are: Mean Absolute Error (MAE), Peak

Signal-to-Noise Ratio (PSNR) and Structural Similarity Image Metric (SSIM) [18]. MAE measures the dispersion derived from the average deviation

$$MAE = \frac{1}{w \times h} \sum_{i=1}^w \sum_{j=1}^h |I_{i,j}^0 - I_{i,j}^n|.$$

The SSIM index is a multiplication of three terms indicating different characteristics of patches within the original and the distorted images: the luminance of the patch, the similarity of the local patch contrasts and the similarity of the local patch structures. The PSNR expresses the ratio between the maximum possible value of a signal and the power of the distorting noise. It is defined by:

$$PSNR = 10 \log_{10} \left(\frac{w \times h \times 255^2}{\sum_{i=1}^w \sum_{j=1}^h (I_{i,j}^0 - I_{i,j}^n)^2} \right),$$

where $I_{i,j}^0$ and $I_{i,j}^n$ represent respectively the original images and the reconstructed images and w, h are respectively the width and height of the image.

5. Results and Comparison Approach

The proposed functions have been tested on different types of images. Images were affected by two different types of noise: salt & pepper noise and Gaussian noise then a discrete form of the nonlinear diffusion was applied. The results of the applied filters are shown in Figures 1, 3, 5, 6, 7 and 8. The obtained results prove that the proposed edge stopping functions preserve the true image edges and other important features while considerably reduce the noise. These results were compared with the following denoising methods: nonlinear second order parabolic PDE based scheme [14], the new Perona-Malik model (SLPM) proposed by Yuan and Wang [5], the two function proposed by Perona and Malik in their original paper [9] and the Total Variation (TV) approach [7]. The results of comparison of the proposed functions H_1, H_2 and H_3 with the above denoising techniques using the PSNR and MAE as a metrics of quality are presented in Table 1 below.



Figure 1: Performance comparison for $\sigma = 0, 14$. Resulting denoised images with the our edge stopping functions after 28 iterations. (a) Noisy image with Gaussian noise ($\mu = 0, 04$; $var = 0, 05$), (b) Results using H_1 , (c) Results using H_2 , (d) Results using H_3 .

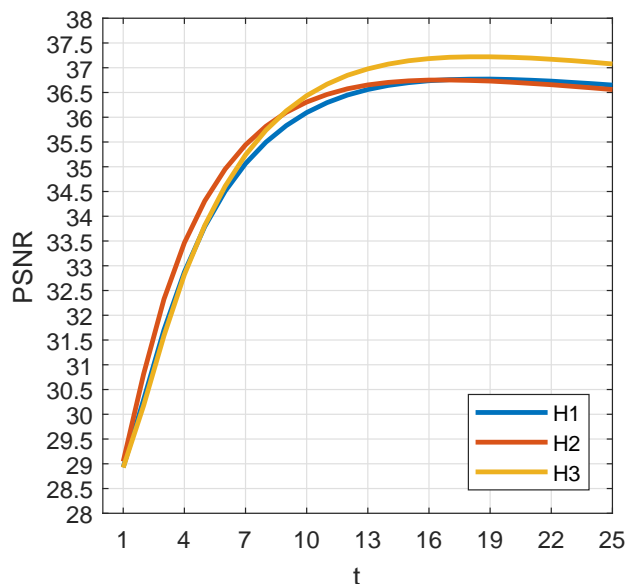


Figure 2: The measured PSNR value for each iteration. Using our edge stopping functions.

In Figures 1 and 3, we tested our proposed functions on two different images affected by Gaussian noise. We used this type of noise at varying density to conform the efficiency of these functions. The performed denoising shows clearly that our edge stopping functions reduce the noise while image edges and the important features remain untouched. In it avoids undesirable effects, such as staircasing effect. We measured the performance of our functions by PSNR and SSIM, the results are displayed in Figures 2 and 4, respectively. From Figures 2 and 4, PSNR and SSIM values for H_3 are higher than H_2 and H_1 , indicating that the performance of function H_3 is better than H_1 and H_2 . This result can also be confirmed by observing the quality of images recovered by H_1 , H_2 and H_3 are shown in Figures 1 and 2.

Table 1: Values of PSNR and MAE calculated from denoising approaches for Elaine image after 20 iterations.

Different denoising approaches	PSNR	MAE
First edge stopping function	38.4535	0.0418
Second edge stopping function	38.4538	0.0417
Third edge stopping function	38.4581	0.0416
2^{nd} -order PDE scheme	37.8458	0.0427
SLPM	38.0604	0.0424
Perona-Malik1	37.2312	0.0451
Perona-Malik2	37.2677	0.0447
TV	37.3739	0.0440

According to Table 1, one can see clearly that the PSNR and MAE values of our functions are greater than PSNR and MAE values for the other different methods. Figure 8 confirms the superiority of the results of our edge stopping functions, which we obtained through denoising Elaine image using our edges stopping functions after 20 iterations. The image is affected by a Gaussian noise with $\mu = 0.04$ and a variance $\sigma = 0.05$.

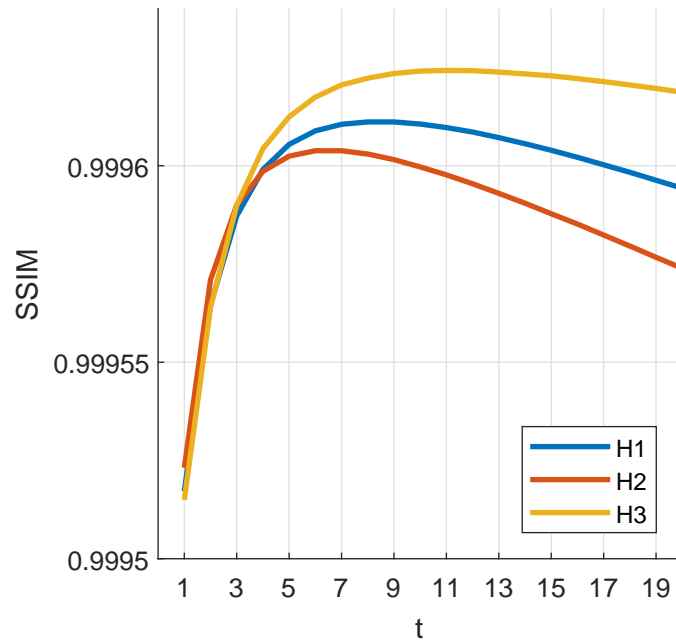


Figure 3: The measured SSIM value for each iteration t . Result between the corrupted and the filtered images for a noisy medical image, using our different functions.

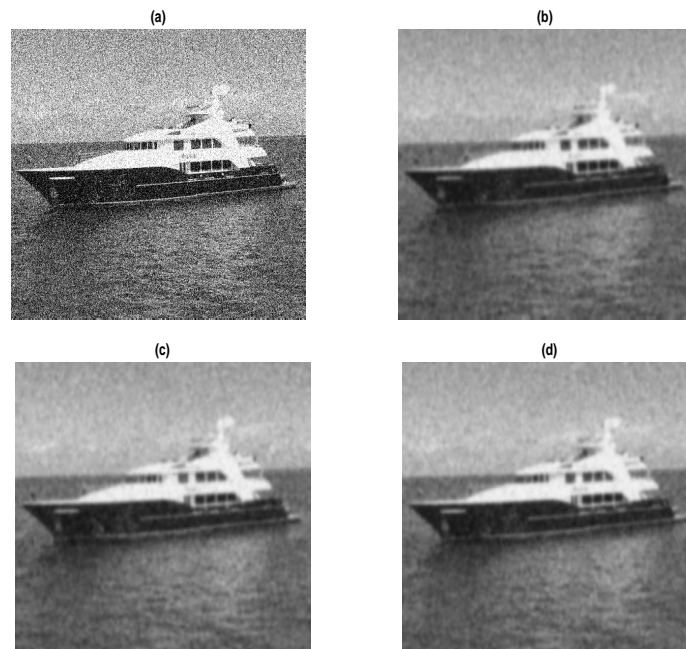


Figure 4: Performance comparison for $\sigma = 0,76$. Resulting denoised images with the our edge stopping functions after 20 iterations. (a) Noisy image with Gaussian noise ($\mu = 0,04$; $var = 0,05$), (b) Results using H_1 , (c) Results using H_2 , (d) Results using H_3 .

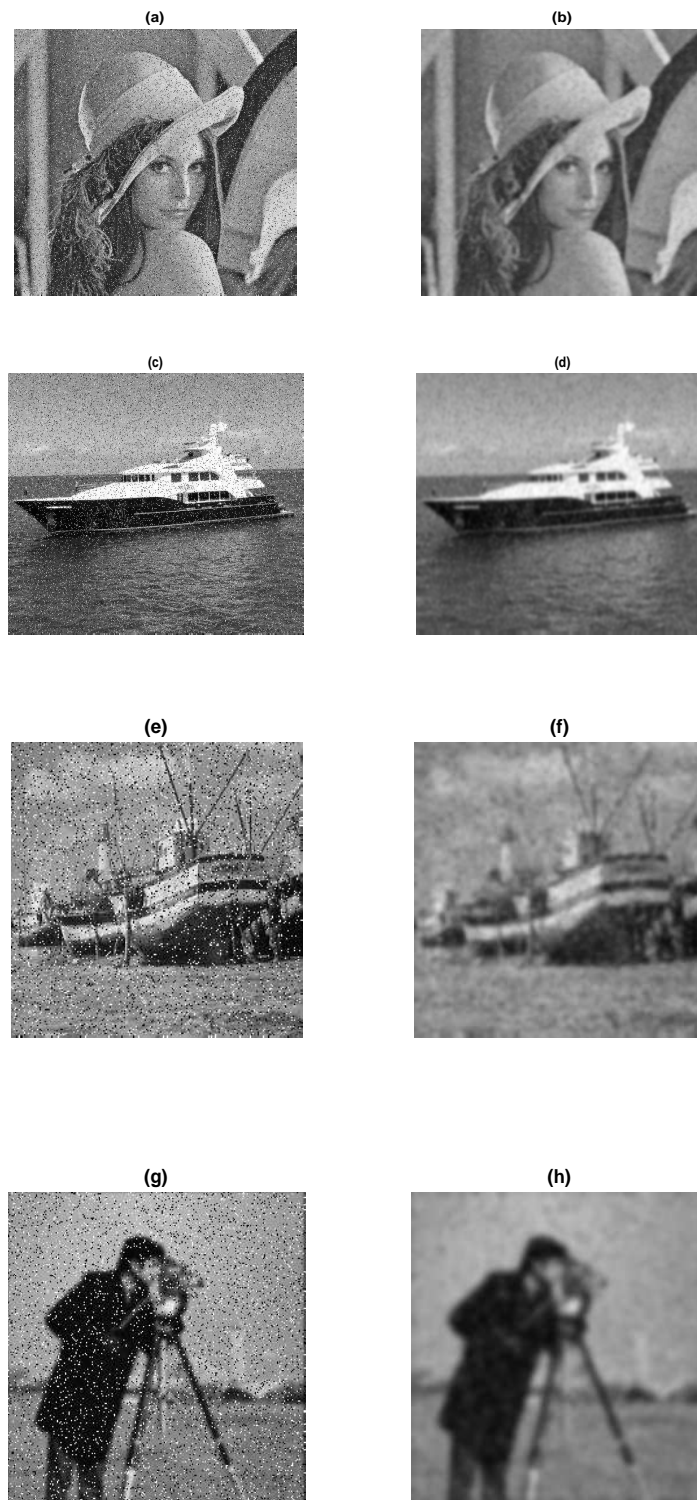


Figure 5: The obtained results using H_1 . (a), (c), (e) and (g) are the noisy images with salt & pepper noise equal to 0.1, (b), (d), (f) and (h) are the restored images.

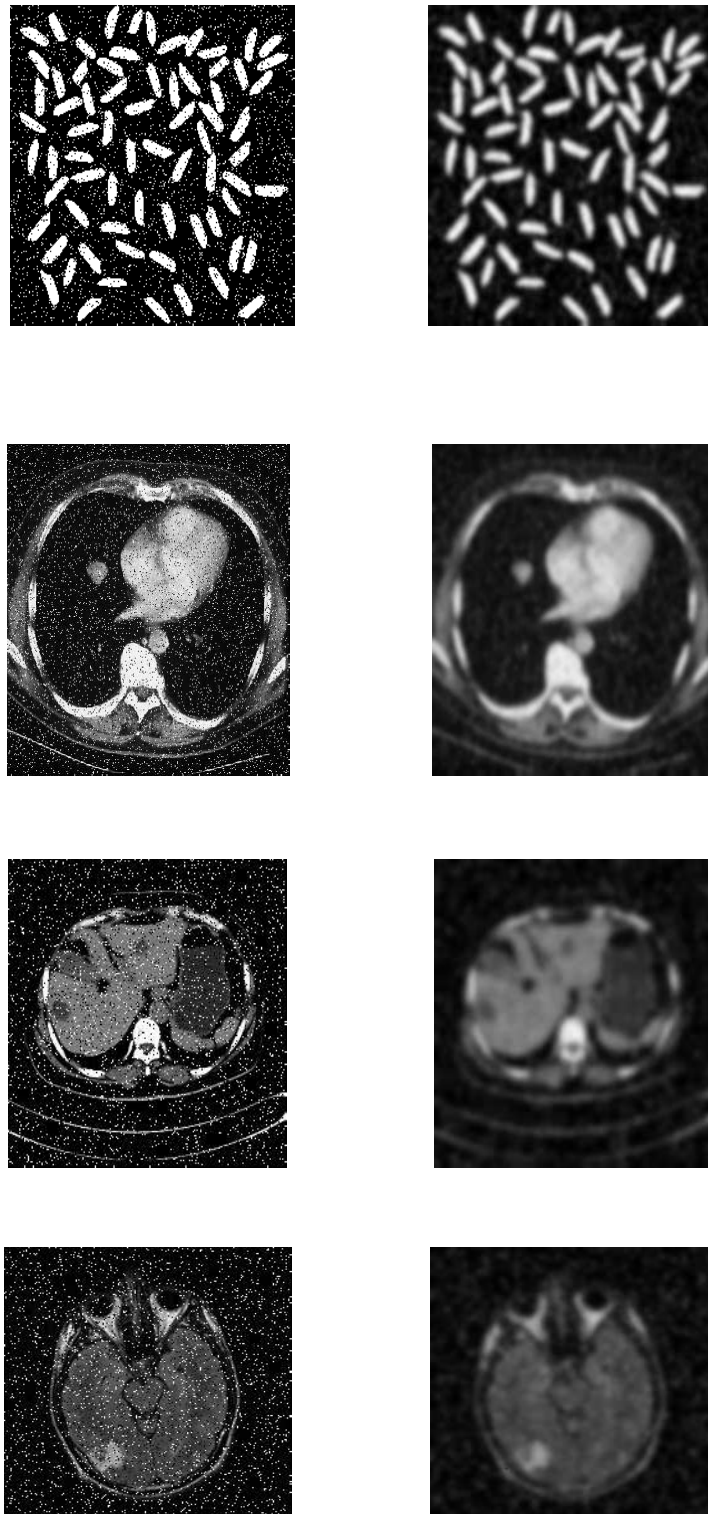


Figure 6: The restoration results using H_2 . In the first column: the noisy images with salt & pepper noise with a density equal to 0.1. The second column: the restored images after.

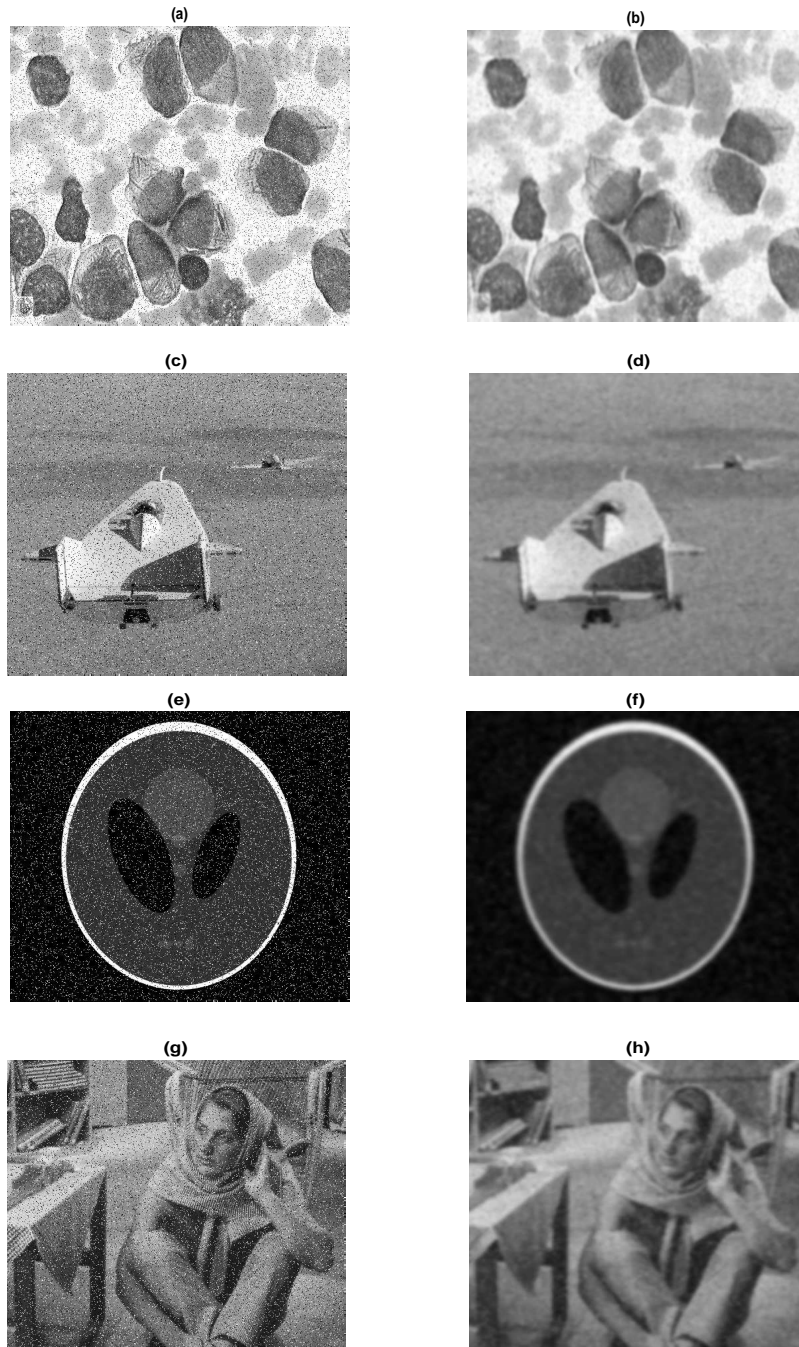


Figure 7: The denoising results using H_3 . (a), (c), (e) and (g) are the noisy images with salt & pepper noise with a density equals to 0.1. (b), (d), (f) and (h) are the denoising images.



Figure 8: The restored images using our edge stopping functions and the existing approaches. The first row: left image is a noisy image, the middle is restored image using H_1 , the right is restored image using H_2 , the second row: left image is restored image using H_3 , the middle is restored image using Perona-Malik1, the right is restored image using Perona-Malik 2. The third row: left image is restored image using TV approach, the middle is restored image using the 2nd – order PDE scheme and the right image is restored image using SLPM model.

6. Conclusion

In this article, we proposed three novel edge stopping functions for image denoising. These edge stopping functions produced better results by removing the image noise without touching the true image edges and other important features compared to existing approaches. In addition the numerical results show that the performance of the diffusion process is significantly improved.

References

1. Catté, Francine and Lions, Pierre-Louis and Morel, Jean-Michel and Coll, Tomeu; *Image selective smoothing and edge detection by nonlinear diffusion*, SIAM Journal on Numerical analysis, 29, No.1, 182-193, (1992).
2. Tian, Haiying and Cai, Hongmin and Lai, Jian-Huang and Xu, Xiaoyin; *Effective image noise removal based on difference eigenvalue* Image Processing (ICIP), 2011 18th IEEE International Conference on, 3357-3360, (2011).
3. Monteil, Jérôme and Beghdadi, Azeddine; *A new interpretation and improvement of the nonlinear anisotropic diffusion for image enhancement* IEEE Transactions on Pattern Analysis and Machine Intelligence, 21, No.9, 940-946, (1999).
4. Weickert, Joachim; *Coherence-enhancing diffusion filtering*, International journal of computer vision, 31, No.2-3, 111-127, (1999).

5. Yuan, Jianjun and Wang, Jianjun; *Perona–malik model with a new diffusion coefficient for image denoising*, International Journal of Image and Graphics, 16,No.2, 1650011, (2016).
6. Liu, Kui and Tan, Jieqing and Su, Benyue; *Adaptive anisotropic diffusion for image denoising based on structure tensor*, Digital Home (ICDH), 2014 5th International Conference on, 111-116, (2014).
7. Rudin, Leonid I and Osher, Stanley and Fatemi, Emad; *Nonlinear total variation based noise removal algorithms*, Physica D: nonlinear phenomena, 60, No.1-4, 259-268, (1992).
8. Black, Michael J and Sapiro, Guillermo and Marimont, David H and Heeger, David; *Robust anisotropic diffusion*, IEEE Transactions on image processing, 7, No.3, 421-432, (1998).
9. Perona, Pietro and Malik, Jitendra; *Scale-space and edge detection using anisotropic diffusion*, IEEE Transactions on pattern analysis and machine intelligence, 12, No.7, 629-639, (1990).
10. Whitaker, Ross T and Pizer, Stephen, M.; *A multi-scale approach to nonuniform diffusion*, CVGIP Image Understanding, 57, 99-99, (1993).
11. Osher, Stanley and Rudin, Leonid, I.; *Feature-oriented image enhancement using shock filters*, SIAM Journal on numerical analysis, 27, No.4, 919-940, (1990).
12. Chen, Shifeng and Liu, Ming and Zhang, Wei and Liu, Jianzhuang; *Edge preserving image denoising with a closed form solution*, Pattern Recognition, 46, No.3, 976-988, (2013).
13. Barbu, Tudor; *Robust anisotropic diffusion scheme for image noise removal*, Procedia Computer Science, 35, No.3, 522-530, (2014).
14. Barbu, Tudor and Moroşanu, Costică; *Image Restoration using a Nonlinear Second-order Parabolic PDE-based Scheme*, Analele Universitatii” Ovidius” Constanta-Seria Matematica, 25, No.1, 48-33, (2017).
15. Kamalaveni, V and Rajalakshmi, R Anitha and Narayanankutty, K. A.; *Image denoising using variations of Perona-Malik model with different edge stopping functions*, Procedia Computer Science, 58, 673-682, (2015).
16. Li, Xiaoping and Chen, Tongwen; *Nonlinear diffusion with multiple edginess thresholds*, Pattern Recognition, 27, No.8, 1029-1037, (1994).
17. Wang, YQ and Guo, Jichang and Chen, Wufan and Zhang, Wenxue; *Image denoising using modified Perona-Malik model based on directional Laplacian*, Signal Processing, 93, No.9, 2548-2558, (2013).
18. Wang, Zhou and Bovik, Alan C and Sheikh, Hamid R and Simoncelli, Eero P.; *Image quality assessment: from error visibility to structural similarity*, IEEE transactions on image processing, 13, No.4, 600-612, (2004).
19. Guo, Zhichang and Sun, Jiebao and Zhang, Dazhi and Wu, Boying; *Adaptive Perona-Malik model based on the variable exponent for image denoising*, IEEE Transactions on Image Processing, 21, No.3, 958-967, (2012).

Hicham Rezgui,

Department of Mathematics, Laboratory of Mathematical Modeling and Numerical Simulation

Badji Mokhtar University, Annaba, Algeria.

E-mail address: hicham.rezgui@univ-annaba.org

and

Messaoud Maouni,

Department of Mathematics,

Laboratory of Applied Mathematics and History and Didactics of Mathematics,

Laboratory of Mathematical Modeling and Numerical Simulation,

Université of 20 août 1955 ,Skikda, 21000, Algeria.

E-mail address: m.maouni@univ-skikda.dz

and

Mohammed Lakhdar Hadji,

Department of Mathematics,

Probability and Statistics Laboratory,

Badji Mokhtar University, Annaba, Algeria.

E-mail address: ml.hadji@yahoo.fr

and

Ghassen Touil,

Department of computer science,

20 août 1955 University, Skikda, Algeria.

E-mail address: g.touil@univ-skikda.dz